Supporting Information

Zhou et al. 10.1073/pnas.1304504110

SI Text

Poly(lactide-coglycolide) (PLGA) nanoparticles loaded with paclitaxel were synthesized by two techniques: brain-penetrating and standard paclitaxel-loaded nanoparticles were spherical and of expected diameters (75 ± 20 nm and 159 ± 38 nm, respectively) (Fig. S1*A*). All nanoparticle fabrications (brain-penetrating and standard) were loaded with paclitaxel, having encapsulation efficiencies of ∼60% and yields of >35%. Controlled-release experiments showed that brain-penetrating and standard PLGA nanoparticles released paclitaxel similarly, with ∼75% of the encapsulated drug released from each formulation over the first 28 d of incubation (Fig. S1*B*). Both brain-penetrating and standard paclitaxel nanoparticles inhibited growth of U87MG in vitro, exhibiting lower IC_{50}s (39 nM and 37 nM, respectively) than free drug (169 nM). None of the blank nanoparticle formulations exhibited cytotoxicity (Fig. S1*C*).

To determine in vivo efficacy, we generated U87MG-derived xenografts in the right striatum of nude rats. Tumor-bearing rats were divided into five groups that received either no treatment ($n = 5$); convection-enhanced delivery (CED) of brain-penetrating, paclitaxel-loaded nanoparticles ($n = 10$); CED of standard, paclitaxel-loaded nanoparticles ($n = 10$); CED of blank (unloaded), brain-penetrating nanoparticles ($n = 5$); or CED of paclitaxel in solution ($n = 10$). Consistent with our previous experience, rats tolerated all procedures well; no periprocedural toxicity was observed in any of the treatment groups. Kaplan–Meier analysis revealed that rats treated with brain-penetrating, paclitaxel-loaded nanoparticles had significant improvements in median survival (46 d) compared with all other groups (38 d for standard nanoparticles, 30 d for free drug, 31 d for blank/unloaded nanoparticles, and 27 d for no treatment; $P < 0.05$ for each comparison) (Fig. S1*D*).

SI Materials and Methods

Chemicals. All chemicals were purchased from Sigma-Aldrich unless otherwise noted.

Cell Culture. Human glioma cell line U87MG was purchased from American Type Culture Collection. Cells were grown in a 37 °C incubator containing 5% CO_2 and cultured in DMEM (Invitrogen) supplemented with 10% FBS (Invitrogen), 100 units/mL penicillin, and 100 μg/mL streptomycin (Invitrogen).

Brain Cancer Stem Cell Cultures from Human Glioblastoma Multiforme Tissue. All studies were approved by the Yale University Institutional Review Boards. Tumor samples classified as glioblastoma multiforme (GBM) based on World Health Organization criteria were obtained from neurosurgical patients at Yale–New Haven Hospital who had provided informed consent. Within 1–3 h of surgical removal, tumors were washed, cut into <1-mm^3 fragments, and enzymatically dissociated into single cells. Digested fragments were filtered using a 70-μm cell strainer (BD Falcon) and collected in culture medium. The GS5 cell line was kindly provided by the Lamszus laboratory (1). All brain cancer stem cell cultures (BCSCs) were collected and cultured in Neurobasal A medium (Invitrogen) supplemented with B27 (Invitrogen), fibroblast growth factor-2 (20 ng/mL; Peprotech), and epidermal growth factor (20 ng/mL; Peprotech). Growth factors were added at least weekly.

SEM. Particle size was characterized by SEM. Samples were mounted on carbon tape and sputter-coated under vacuum with gold in an argon atmosphere using a Dynavac Mini Coater set at 40 mA current (Dynavac). SEM was carried out using a Philips XL30 SEM and a LaB electron gun with an accelerating voltage of 3 kV. Mean particle diameters and size distributions were determined by image analysis of ∼200 particles using ImageJ (National Institutes of Health). The same images were used to qualitatively assess particle morphology.

Characterization of Nanoparticle Loading. To determine the loading and encapsulation efficiency of coumarin-6 (C6) nanoparticles, 3–5 mg of nanoparticles were dissolved in 1 mL of DMSO at room temperature. Loading of C6 in the nanoparticles was quantified based on the solution's fluorescence intensity (excitation 444 nm and emission 538 nm) using a spectrophotometer (Spectromax M5; Molecular Devices). Blank nanoparticles were used for background control. Paclitaxel loading was quantified using HPLC as previously reported (2). The same approach was used to characterize loading of dithiazanine iodide (DI) in nanoparticles, except that the concentration of DI was determined based on its absorbance at 655 nm.

In Vitro Controlled Release. Nanoparticles (3–5 mg) were suspended in 1 mL of PBS (pH 7.4) and incubated at 37 °C with gentle shaking (70 rpm). Release of C6, paclitaxel, or DI was monitored at several time points over a 4-wk period. At each sampling time, the nanoparticle suspension was centrifuged for 15 min at 21,000 × *g*. The supernatant was removed for quantification of C6, paclitaxel, or DI and replaced with an equivalent volume of PBS for continued monitoring of release. Detection of C6, paclitaxel, or DI was conducted using the methods described above.

Fluorescence-Based Imaging of Nanoparticle Distribution in Rat Brain. All procedures involving animals were approved by the Yale University Institutional Animal Care and Utilization Committee (IACUC). Female athymic (NCr-*nu*/*nu*) nude rats were maintained in a sterile environment. Rats were anesthetized with ketamine/xylazine solution via i.p. injection and given analgesic. The scalp was prepped with betadine and alcohol. The rat was then placed in a stereotactic head frame. A midline incision was made and a 1.5-mm-diameter hole was drilled in the skull 3 mm lateral and 0.5 mm anterior to the bregma. The right striatum was targeted. A 26G Hamilton syringe, with 28G stepdown inner cannula, was inserted to a depth of 5 mm. The tissue was allowed to equilibrate mechanically for 5 min. Subsequently, 20 μL of nanoparticles (100 mg nanoparticles/mL solution) ($n = 4$/group) was infused (V_i) continuously at a rate of 0.667 μL/min. Following infusion, the syringe was left in place for 5 min to allow for equilibration. For distribution studies, animals were killed 30 min postinfusion; the brains were harvested and frozen.

Nanoparticle distribution was quantified using previously described methods (3). Specifically, each brain was serially sectioned into 150-μm slices on a cryostat. The distribution of nanoparticles in the slices was captured on a fluorescence stereoscope (Lumar V.12; Carl Zeiss) using a Cy3 filter. The exposure time was optimized to achieve maximum dynamic range at the infusion site while simultaneously avoiding saturation. Exposure time for each nanoparticle group was individually optimized, to adjust for differences in loading between nanoparticle groups. Within each group of nanoparticles, the exposure time was held constant. The distribution volume (V_d) of the nanoparticles was calculated using a custom Matlab 7.2 (MathWorks) script, which generated a binary image from the grayscale images and calculated the area of particle penetration. The threshold for the binary operation was

10% of the maximum fluorescent intensity. The total V_d was calculated by multiplying the distribution area in each slice by the slice thickness (150 μm) and summing the volumes of all slices.

Synthesis of *N*-(4-[^{18}F]fluorobenzyl)propanamido-PEG$_4$-Biotin Nanoparticles. *N*-(4-[^{18}F]fluorobenzyl)propanamido-PEG$_4$-Biotin ([^{18}F]NPB4) was prepared as previously described (4), with 28 ± 14% radiochemical yield, >98% radiochemical purity, and 1–2 mCi/nmol specific activity. In preliminary experiments, [^{18}F]NPB4 was conjugated to avidin surface-modified PLGA nanoparticles by incubating 7 mg of nanoparticles with ∼0.6 mCi of [^{18}F]NPB4 for 1 h at room temperature. When this solution was centrifuged to pellet the nanoparticles, less than 1% of the total added radioactivity was detected in the wash. We estimated that <1% of available avidin sites on the nanoparticles were occupied by the [^{18}F]NPB4. Each rat received a total dose of 100–300 μCi.

PET-Based Imaging of Nanoparticle Distribution in Rat Brain. For noninvasive imaging studies, Sprague Dawley rats (n = 5) were anesthetized with ketamine/xylazine and a 26G guide cannula was placed in the skull (Plastics One) to enable nanoparticle infusions while data collection was ongoing. The right striatum was targeted. The guide cannula was secured to the surface of the skull with dental cement (Henry Schein) and surgical screws. Once in the scanner, rats were maintained on isofluorane anesthesia [2% (vol/vol)], and an infusion needle was threaded through the cannula to the target brain region. Emission data were collected during the infusion and for 30 min after completion with a Focus 220 small animal PET scanner (Siemens Medical Solutions). A transmission scan (^{57}Co source, 9 min) was collected before the emission scan. Rats were killed immediately after the scan and frozen in liquid nitrogen for later tissue sectioning and fluorescence microscopy. PET data were binned into 0.5- to 10-min frames and reconstructed with the ordered subset expectation maximization algorithm, with corrections for attenuation, decay, randoms, and scatter. The resulting pixel size was 0.949 × 0.949 × 0.796 mm, with an effective image resolution of ∼1.5 mm. Radial concentration profiles were extracted from each data frame and thresholded to 10% of the maximum value to determine the spatial volume of distribution.

Fluorescence-Based Imaging of Nanoparticle Distribution in Pig Brain. Nanoparticle infusions were performed in the striatum of Yorkshire pigs (n = 4) to evaluate V_d in a large animal model. Pigs were anesthetized with ketamine/xylazine, intubated, and maintained with isofluorane/oxygen/NO_2. The head was positioned such that the horizontal zero plane passed through bregma and was parallel to a line between the upper margin of the infraorbital ridge and the upper margin of the external auditory meatus. The scalp was prepped with betadine and alcohol. A linear midline incision was made and a 1.5-mm-diameter hole was drilled in the skull 11 mm lateral to bregma. A 26G Hamilton syringe, with 28G stepdown inner cannula, was inserted to a depth of 28 mm. The tissue was allowed to equilibrate mechanically for 5 min. Subsequently, 337.5 μL of nanoparticle solution were continuously infused at a rate of 0.5 μL/min for 30 min, 0.75 μL/min for 30 min, and 1 μL/min for 300 min. Following infusion, the syringe was left in place for 120 min, after which it was removed. Animals were subsequently killed; the brains were harvested, frozen, and sectioned as described above. Nanoparticle distribution was quantified using the methods described above. Exposure time was held constant between all animals.

Cell Proliferation Assays. For primary screening, a slightly modified thiazolyl blue tetrazolium bromide (MTT) assay was used to quantify the effects of drugs on cell proliferation. Briefly, cells were cultured in 96-well plates (Falcon). Three (for BCSC studies) or six (for U87MG studies) days after treatment, medium was removed and replaced with fresh medium containing 10% MTT [3-(4,5-dimethylthiazol-2-yl)-2,5-diphenyl tetrazolium bromide] (Sigma) solution (4.14 mg/mL). Four hours after incubation at 37 °C, all of the media was removed. Formazan was dissolved in DMSO and the OD was measured at 590 nm. The relative inhibition on growth was determined using the following formula: Growth inhibition = (control OD − sample OD)/control OD.

Proliferation was also assessed and IC_{50} calculated using AlamarBlue (Invitrogen) fluorescence. Briefly, cells were plated at subconfluent concentrations in black clear-bottomed 96-well plates (Falcon) with drug concentrations spanning eight orders of magnitude. Three or six days postplating (as above), AlamarBlue was added at the manufacturer's recommended concentration. Cells were incubated at 37 °C for 200 min and quantified (excitation 544 nm and emission 590 nm). Fluorescence measurements were corrected for background media and drug fluorescence and normalized to the mean of vehicle measurements. IC_{50} values were determined using four-parameter logistic modeling using normalized point estimates.

Sphere Formation Assay. BCSCs were plated as single-cell suspensions of five cells per microliter in 48-well plates (Falcon). Cells were treated with 1 μM drug or equivalent concentration of DMSO. Growth factor was supplemented on day 5. Wells were counted on day 7. Colonies containing more than five cells were considered to be spheres. Percent inhibition was calculated as (Control number of spheres – sample number of spheres)/control number of spheres.

Flow Cytometry. BCSCs were plated as single-cell suspensions in six-well plates with 100 nM drug or DMSO. Three days after plating, suspensions were collected and flow cytometry performed. Briefly, following reconstitution in 0.5% BSA in PBS (wt/vol), dissociated cells were washed in cold PBS and subsequently incubated with biotin-conjugated anti-CD133 (PROM1) antibody (Miltenyi Biosciences). Suspensions were incubated with avidin-conjugated AlexaFluor 488 (Invitrogen) and read on a FACScan flow cytometer (BD Biosciences). Geometric means were calculated in FlowJo (TreeStar, Inc.), corrected for background (secondary only), and normalized to DMSO-only treated cells.

1. Günther HS, et al. (2008) Glioblastoma-derived stem cell-enriched cultures form distinct subgroups according to molecular and phenotypic criteria. *Oncogene* 27(20):2897–2909.
2. Liu Y, Pan J, Feng SS (2010) Nanoparticles of lipid monolayer shell and biodegradable polymer core for controlled release of paclitaxel: Effects of surfactants on particles size, characteristics and in vitro performance. *Int J Pharm* 395(1-2):243–250.
3. Neeves KB, Sawyer AJ, Foley CP, Saltzman WM, Olbricht WL (2007) Dilation and degradation of the brain extracellular matrix enhances penetration of infused polymer nanoparticles. *Brain Res* 1180:121–132.
4. Zheng MQ, et al. (2011) PEG-Biotin labeled nanoparticles for tracking drug delivery and tumor therapy. *J Nucl Med* 52(Suppl 1):417.

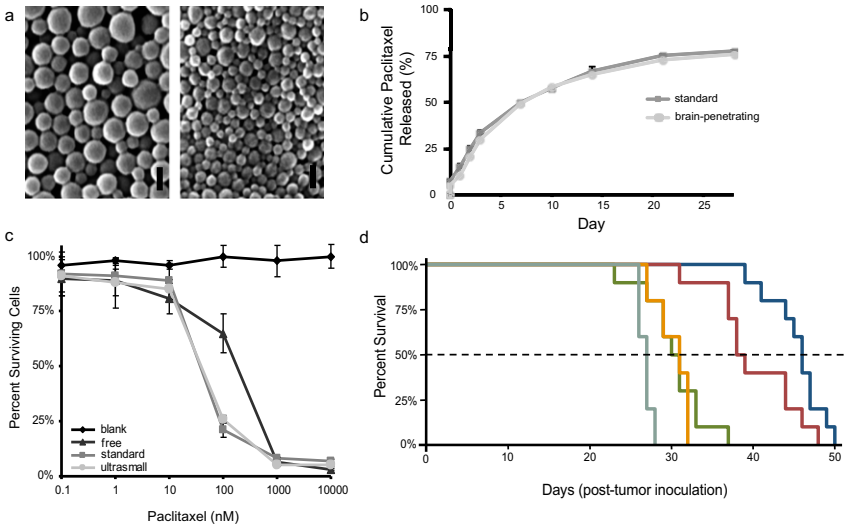

Fig. S1. Synthesis and antitumor effects of paclitaxel-loaded nanoparticles on U87MG cell culture and intracranial tumors in the rat. (*A*) Morphology of standard (*Left*) and small (*Right*) nanoparticles used in studies. (Scale bar, 200 nm.) (*B*) Controlled release of paclitaxel from nanoparticles. (*C*) Effects of free paclitaxel and paclitaxel-loaded nanoparticles on U87MG cell proliferation, in vitro. (*D*) Kaplan–Meier survival curves for tumor-bearing rats with indicated treatments: blue line, brain-penetrating paclitaxel nanoparticles (NPs) (median survival 46 d); red line, standard paclitaxel NPs (median survival 38 d); green line, free paclitaxel (median survival 30 d); yellow line, blank NPs (median survival 31 d); gray line, no treatment (median survival 27 d). Rats treated with brain-penetrating, paclitaxel-loaded NPs had statistically significant improvements in median survival compared with all other groups ($P < 0.05$ for each comparison).

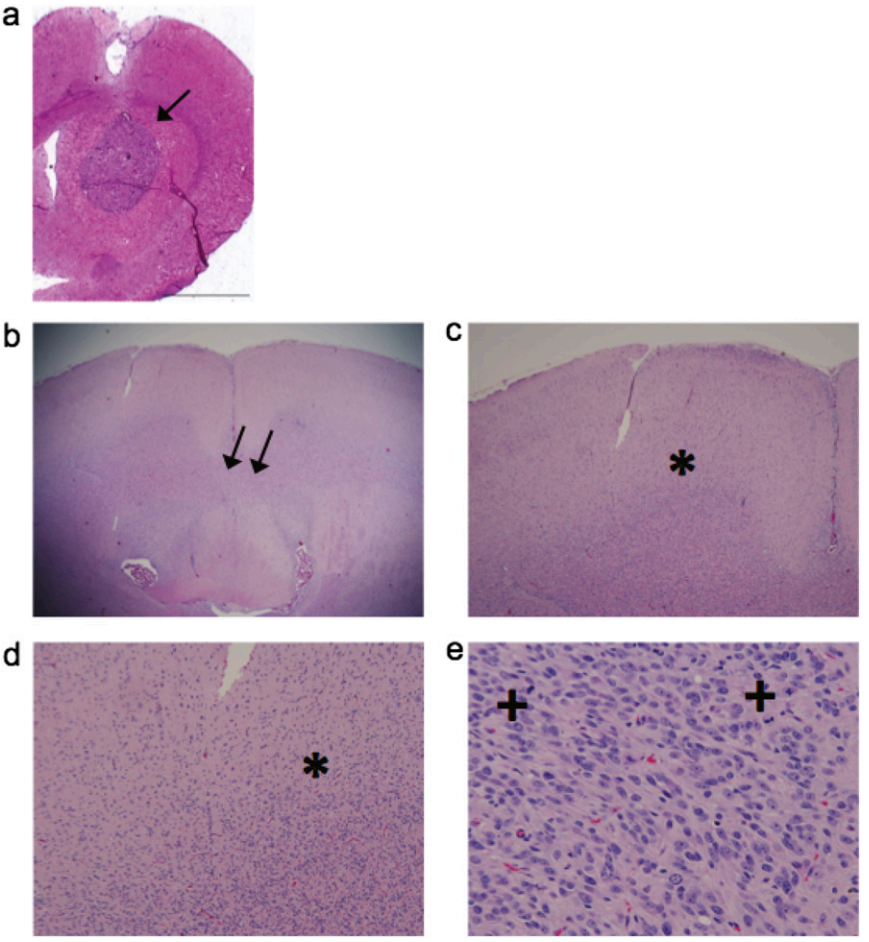

Fig. S2. H&E staining of tumors derived from U87MG cells and BCSCs. (*A*) Implantation of U87MG results in solid tumor formation (arrow) in the rat brain. (*B–E*) Implantation of glioma stem cells (GS5) into the striatum of a nude rat results in diffuse tumor formation. H&E staining demonstrates a highly cellular, infiltrative tumor (asterisk) with invasion of the corpus callosum (arrows) and spread to the contralateral hemisphere. Numerous mitotic figures (+) are noted within a single high-power field. These histopathologic findings are highly similar to those found in human GBM.

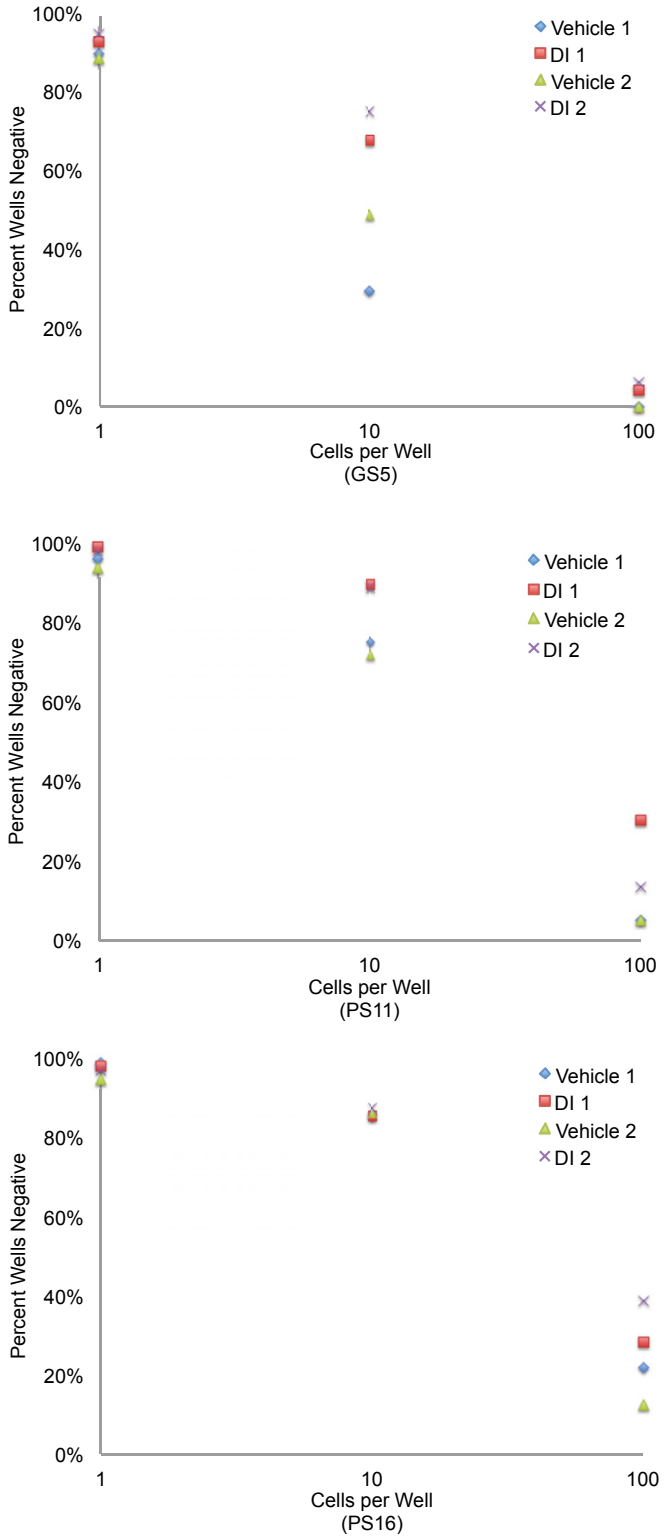

Fig. S3. Inhibition of BCSC self-renewal by DI, as determined by in vitro limiting dilution assays. To assess the self-renewal capacity of these cells when treated with DI, we used a pretreatment strategy as reported by Diamandis et al. (1) but with the addition of a third cell plating density. Pretreatment was used to ensure that what we were observing was not simply cell killing. Briefly, cells were grown in T125 flasks under previously described conditions. Either DI or vehicle solvent DMSO was added to the flask to a final concentration of 100 nM. In accordance with Diamandis et al. (1), cells were further incubated for 1 wk. At the end of 1 wk, the surviving cells were centrifuged and resuspended in non-drug-containing medium. Following TrypanBlue viability assessment, cells were aliquoted and diluted to the following concentrations: one cell per microliter, one cell per 10 μL, and one cell per 100 μL. Three separate 96-well plates were used, one for each concentration. One hundred microliters of each suspension was added to each well of a corresponding 96-well plate. Therefore, 96 wells were evaluated for each set of experimental conditions; in sum >3,000 wells were evaluated. Growth factor was supplemented on day 4 of the experiment. For counting, plates were retrieved from the incubator on day 7 and evaluated under 4× magnification. The total number of neurospheres was

Legend continued on following page

noted for each well. For our purposes, "neurosphere" was defined as a tight group of more than eight cells. The total number of neurospheres for each plate was calculated. Raw neurosphere counts were normalized to the most densely-plated vehicle-treated group. Despite cell line differences in neurosphere formation, a decrease in self-renewal by ~50% was noted following DI pretreatment at all plating densities. The experiment was repeated with similar findings noted.

1. Diamandis P, et al. (2007) Chemical genetics reveals a complex functional ground state of neural stem cells. *Nat Chem Biol* 3(5):268–273.

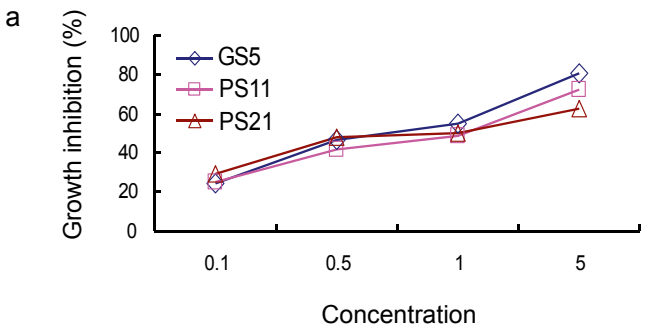

b

Control	1uM	5uM
114	2	1

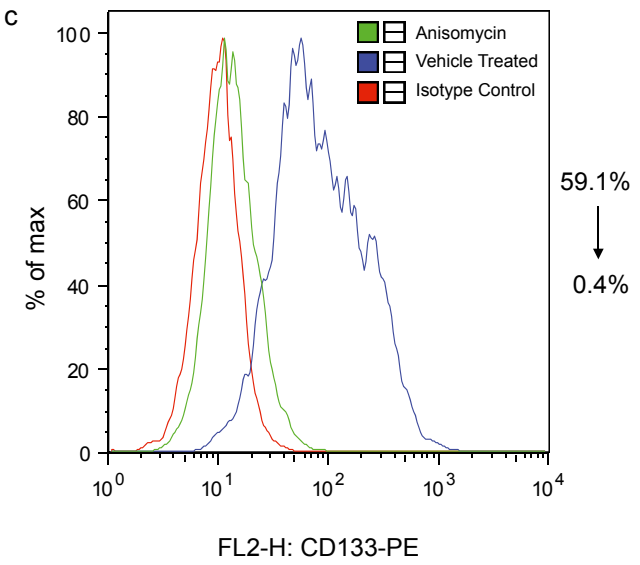

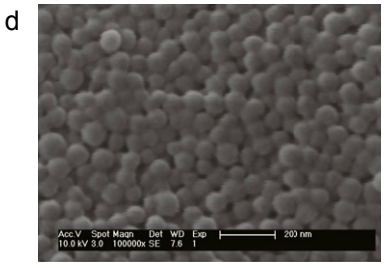

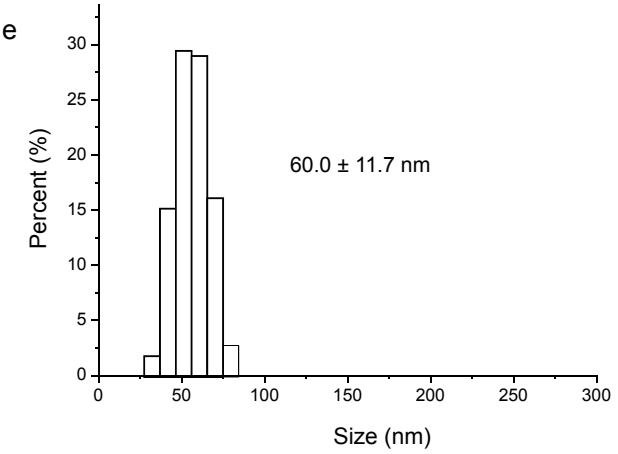

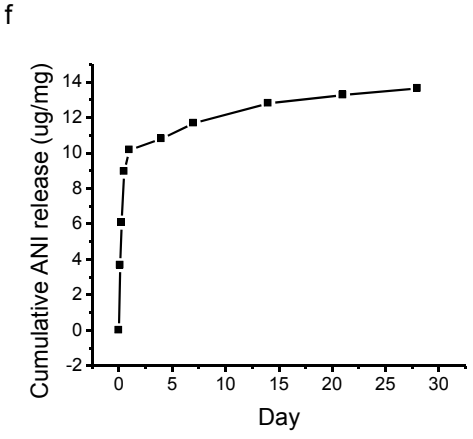

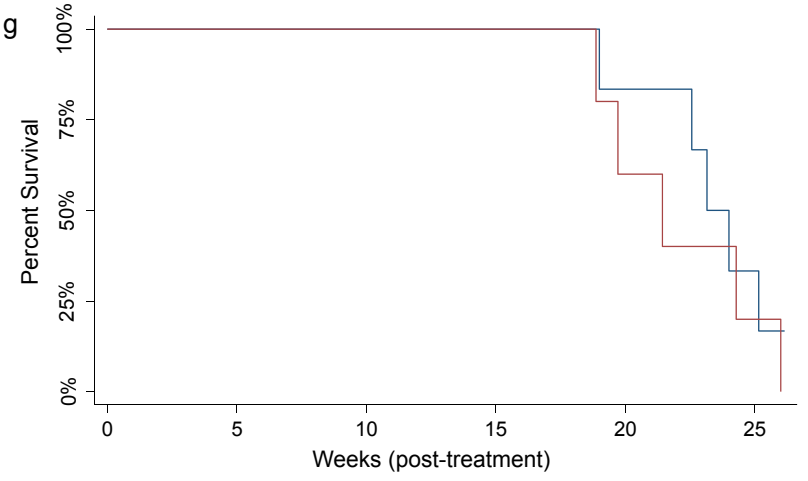

Fig. S4. Evaluation of anisomycin on BCSCs in vitro and in vivo. (*A*–*C*) In vitro evaluation of anisomycin on BCSCs. (*A*) Anisomycin treatment inhibited BCSC proliferation. Cell proliferation was determined using the standard MTT assay described in the main text. (*B*) Treatment with anisomycin at 1 or 5 μM inhibited BCSC sphere formation. Detailed methods for the sphere formation assay are found in the main text, with an inoculation of 500 cells. Of note, the BCSC line PS11 was used in this evaluation. (*C*) Treatment with anisomycin at 1 μM decreased the CD133+ population in the BCSC line PS11, as determined by flow cytometry. (*D*–*F*) Characteristics, including (*D*) morphology, (*E*) size distribution, and (*F*) controlled-release profile of brain-penetrating NPs loading with anisomycin. (*G*) Kaplan–Meier survival curves for tumor-bearing rats with indicated treatments: blue line, control NPs (n = 6); red line, brain-penetrating anisomycin NPs (n = 6).

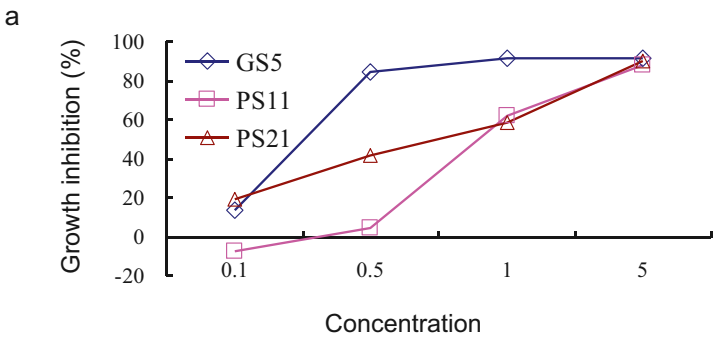

b

Control	1uM	5uM
114	5	3

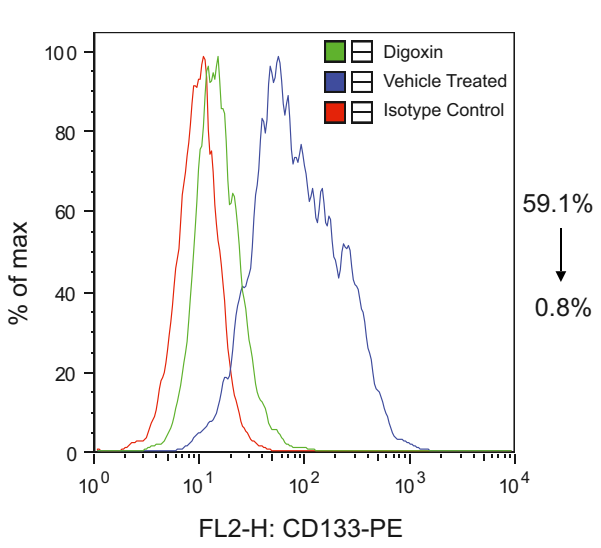

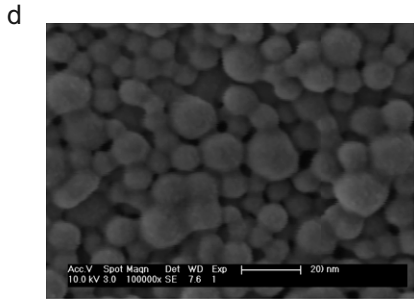

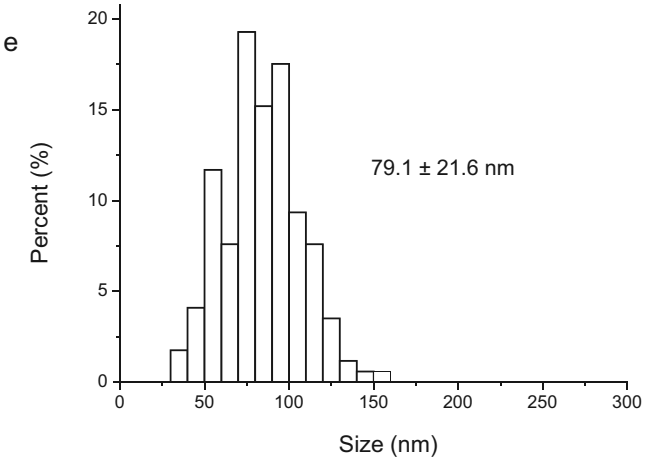

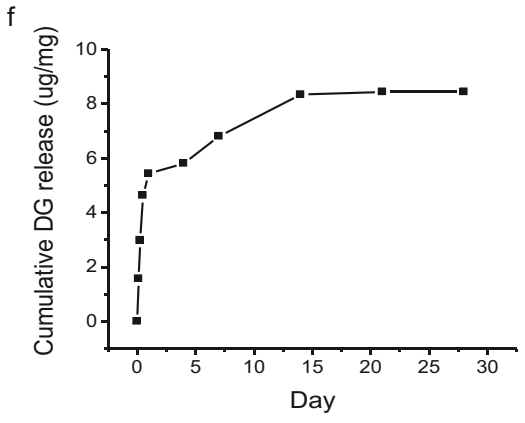

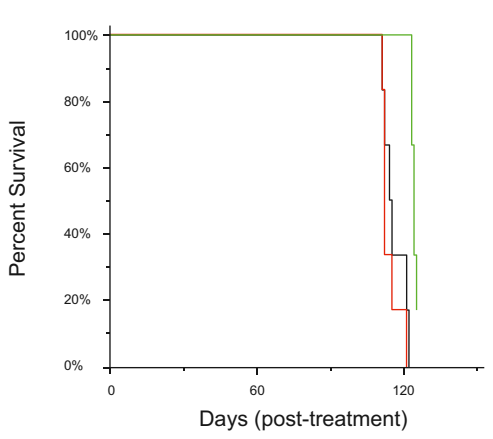

Fig. S5. Evaluation of digoxin on BCSCs in vitro and in vivo. (*A–C*) In vitro evaluation of digoxin on BCSCs. (*A*) Digoxin treatment inhibited BCSC proliferation. (*B*) Treatment with digoxin at 1 or 5 μM inhibited BCSC sphere formation. Of note, the BCSC line PS11 was used in this evaluation. (*C*) Treatment with digoxin at 1 μM decreased the CD133+ population in the BCSC line PS11, as determined by flow cytometry. (*D–F*) Characteristics, including (*D*) morphology, (*E*) size distribution, and (*F*) controlled-release profile of brain-penetrating NPs loaded with digoxin. (*G*) Kaplan–Meier survival curves for tumor-bearing rats with indicated treatments: black line, no treatment ($n = 6$); red line, control NPs ($n = 6$); green line, brain-penetrating digoxin NPs ($n = 6$).

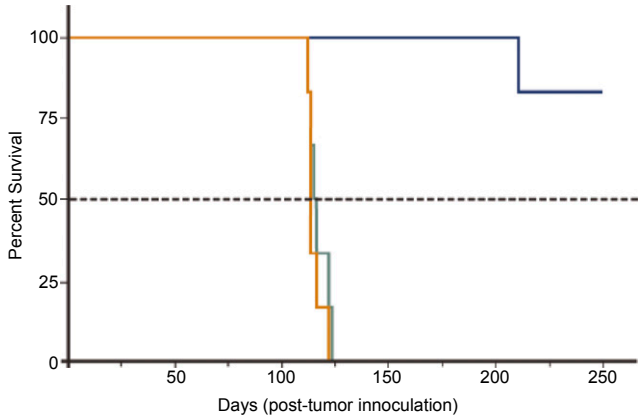

Fig. S6. Replicate of experiment described in Fig. 6. Kaplan–Meier survival analysis of tumor-bearing rats with indicated treatments: blue line, DI brain-penetrating NPs (median survival >250 d); gray line, no treatment (median survival 113 d); yellow line, blank NPs (median survival 115.5 d).

Table S1. Mean hydrodynamic diameter of nanoparticles of different formulations in PBS measured by Zetasizer

		Reconstituted after lyophilization	
Nanoparticles	Size before lyophilization, nm	Cryoprotectant	Size, nm
EA small	165.3	None	259.7
		Trehalose	171.9
EA standard	181.3	None	259.1
		Trehalose	190.8
EA large	189.4	None	236.9
		Trehalose	192.4
DCM small	217.0	None	237.0
		Trehalose	210.6
DCM standard	321.8	None	589.1
		Trehalose	353.5
DCM large	343.7	None	590.8
		Trehalose	390.3

Nanoparticles were synthesized using two different solvents, ethyl acetate (EA) and dichloromethane (DCM). Standard-sized and small nanoparticles were fabricated as described previously. Trehalose was added as a cryoprotectant, as described previously. Nanoparticle size was measured before and after lyophilization. To measure the size of nanoparticles following lyophilization, the nanoparticles were resuspended in PBS and subjected to measurement after brief sonication using a water bath sonicator (2510; Branson).

Table S2. IC_{50} of candidate drugs on GS5 cells

No.	Compound name	IC_{50}, μM
1	Quinacrine	2.7
2	Acriflavine hydrochloride	3.0
3	Cytarabine	0.8
4	8-Hydroxyquinidine	2.7
5	Digoxin	0.3
6	Dithiazanine iodide	0.3
7	Neocuproine	0.2
8	Anisomycin	0.3
9	*p*-aminophenethyl-*m*-trifluoromethylphenyl pierazine	0.9
10	Betamethasone	25.9
11	Chlorpheniramine	40.4
12	Proscillaridin A	0.1
13	Falnidamol	22.0
14	8-Quinolinol hemisulfate	3.0
15	Ammonium pyrrolidinedithiocarbamate	3.3
16	Iron(II) sulfate heptahydrate	32.1
17	Hydroxocobalamin hydrochloride	32.1
18	Glycocyamine	33.9
19	Calcium propionate	29.5
20	Miltefosine	27.8
21	Emetine	0.3
22	Cladribine	3.4
23	Saponin	8.9
24	Parthenolide	3.0
25	Bromocriptine	9.1
26	Hycanthone	5.6
27	Prochlorperazine dimaleate	5.6
28	Astemizole	3.2
29	Harmine	19.3
30	Cephradine	38.5
31	Thioguanine	4.6
32	6-Mercaptopurine monohydrate	7.8